Hall D Cosmic Ray Test Stand Chamber Calibrations

July 2, 2004

Daniel S. Carman
Department of Physics
Ohio University
Athens, OH 45701, USA

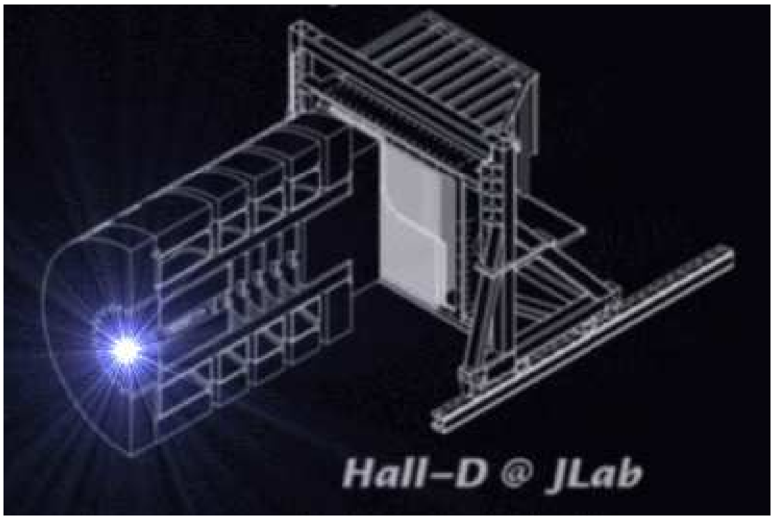

Contents

Abstract

This document represents a compendium of information regarding the calibration procedures and diagnostics for the cosmic ray test stand chambers that will be used for initial study and calibration of the GlueX/Hall D Forward Drift Chamber prototype. This document is expected to evolve and expand as the procedure is carried out and the calibration process continues. Errors and omissions should be sent to the author at carman@jlab.org.

1 Cosmic Ray Test Stand

A set of 19 wire chambers have been borrowed from IUCF in order to put together a cosmic ray test stand at Jefferson Laboratory. This test stand, which is still in the process of being configured, will be used to define tracks through the GlueX/Hall D Forward Drift Chamber (FDC) prototype chamber. A separate test plan for the FDC prototype chamber has been written and entered as GlueX Note 68 [1].

A schematic drawing of the layout of the cosmic ray test stand is shown in Fig. 1. This system employs multiple layers of drift chambers above and below the FDC prototype chamber to precisely define the trajectory of an incident charged particle track that can be used to compare against the position measured in the FDC prototype. This position difference represents a convolution of the resolution of the test stand and of the FDC prototype.

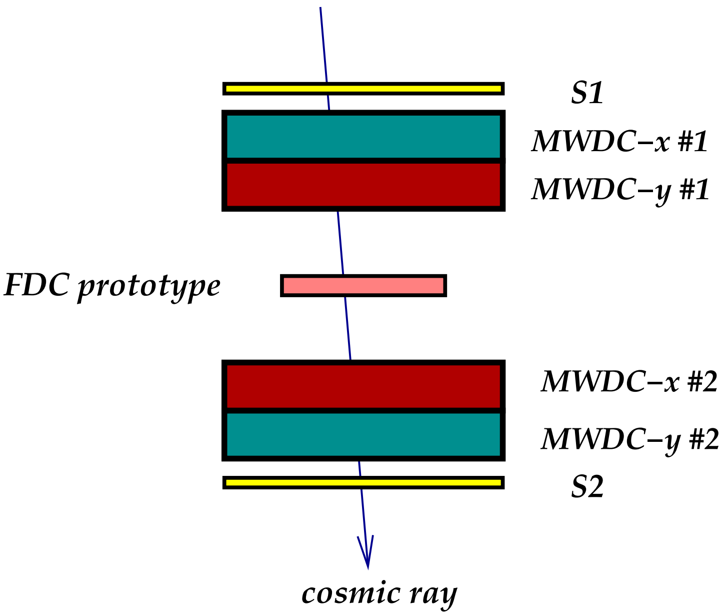

Figure 1: Schematic drawing of the cosmic-ray test stand being used for the FDC prototype resolution studies. Here S1 and S2 represent scintillators used to trigger the readout.

The configuration of the test stand includes two X layers and two Y layers above the FDC prototype and a matching set of four layers below. This system, once properly calibrated, should be capable of defining a track to roughly 200 μm at the location of the FDC prototype.

Each of the 19 1-m long test stand chambers is constructed from an extruded aluminum case. A cross-sectional view of each chamber is shown in Fig. 2. Inside each chamber there are 15 cells, 8 over 7, offset by one half a cell spacing to help reduce the left/right ambiguity (see Section 2). Each cell is 1 in $\times$ 1 in with a single anode wire running down its length. The chambers were designed to operate with the anode wire at positive high voltage with a grounded cathode. The biasing is handled by a simple circuit board mounted on one end of the chamber. The signal readout board, mounted on the other end of the chamber, is read out by a LeCroy 2735 preamplifier/discriminator card [2] which provides a differential ECL signal at its output. Each card is connected to a FASTBUS 1877 TDC via a 50-ft long twisted-pair cable. Preamplifier power is provided by a dedicated power distribution center.

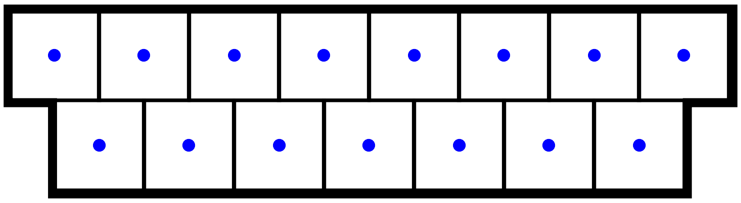

Figure 2: Cross section of one of the extruded aluminum test stand chambers. Each 1-m long chamber is 8 in wide by 2 in high. The anode wires are represented by the blue dots at the center of each square drift cell.

The chambers were transported to JLab in July 2003. After they were unpacked, they were fully re-conditioned and setup in the EEL building in the configuration shown in Fig. 3. Fig. 4 shows the electronics layout as of June 2004, which includes the preamplifier power distribution center (top), along with CAMAC, NIM, and FASTBUS crates.

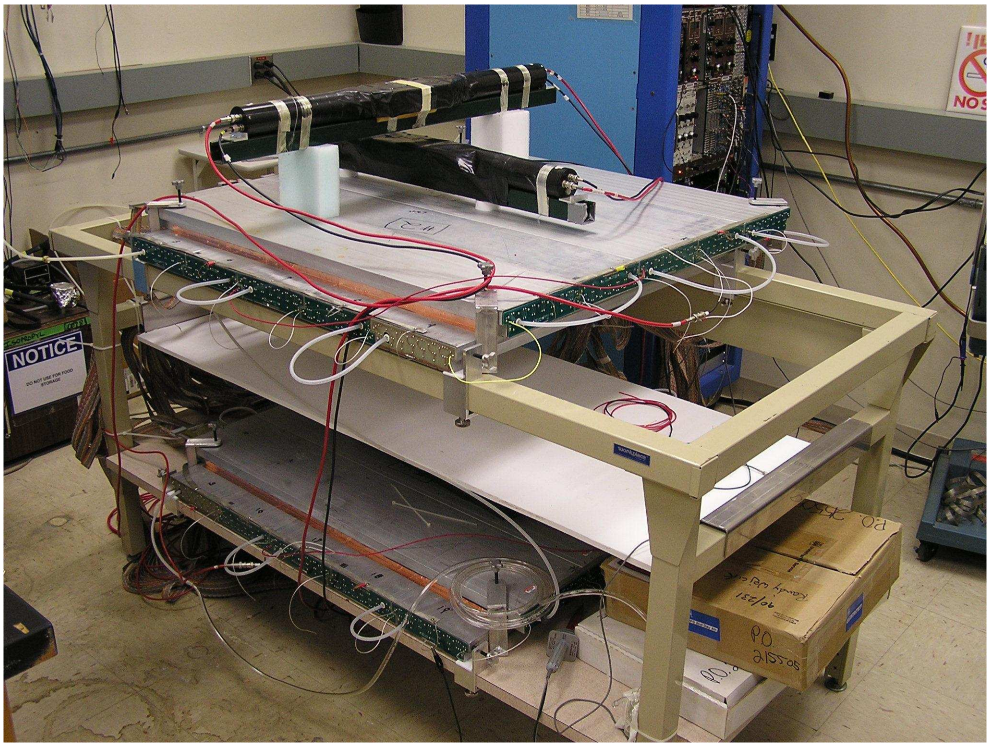

Figure 3: Cosmic ray test stand currently set up in the EEL building at JLab.

The chamber conditioning and preliminary studies have been accomplished using a 90% Argon - 10% CO_2 gas mixture. This mixture is employed as it is non-flammable, however, the mixture does have a fairly high saturated drift velocity (∼40-50 μm/ns) and an operation plateau of several hundred volts before breakdown occurs. Additionally, it provides good efficiency, adequate resolution, and reasonable collection times. A crude plateau was completed showing the chambers were reasonably efficient at ∼2100 V. The discriminator threshold was set at -3.5 V to help reduce the sizeable level of noise present. The studies were

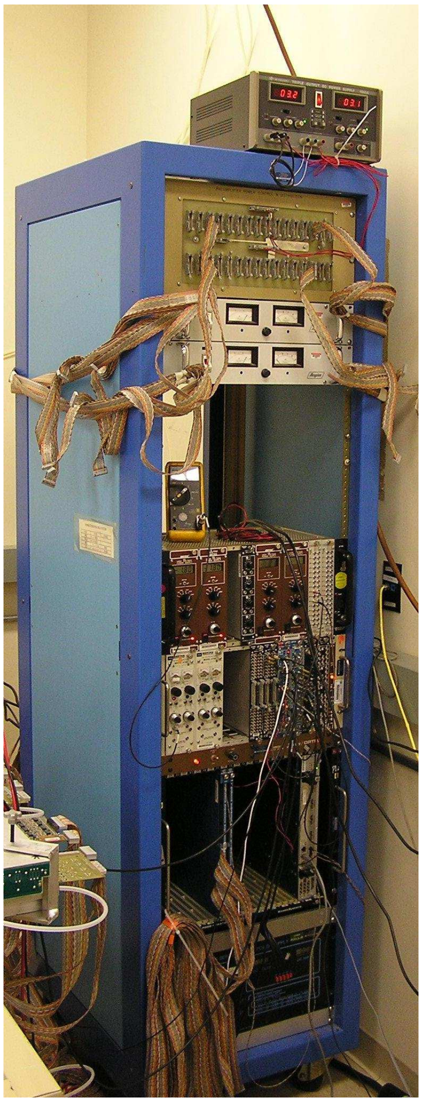

Figure 4: Cosmic ray test stand electronics set up in the EEL building at JLab.

completed without bubbling the chamber gas through propanol as the folks at IUCF advised (none was available at the time of our initial studies). An alcohol refrigeration system with thermostat was brought from IUCF and is available for use.

2 Charged Particle Tracking

Each Multi-Wire Drift Chamber (MWDC) measures the distance from the anode wire to the crossing point of the incident ion in the plane of the anode wires (provided a suitable electric field is defined). In order to infer the position of the incident ion, it is necessary to resolve the left/right position ambiguity. This ambiguity arises in all drift chambers due to the fact that it cannot be directly inferred from the drift time information alone which side of the anode wire the incident ion passed. One method of resolving these ambiguities requires the use of multiple drift chambers. Fig. 5 shows the possible charged particle tracks for the representative case of two identical drift chambers. For the case of a two-point fit, the track reconstruction algorithm would indicate that each of the four possible tracks considered was equally valid. To further reduce these ambiguities, neighboring planes can be offset by half a drift cell spacing (as is the case with the test stand chambers).

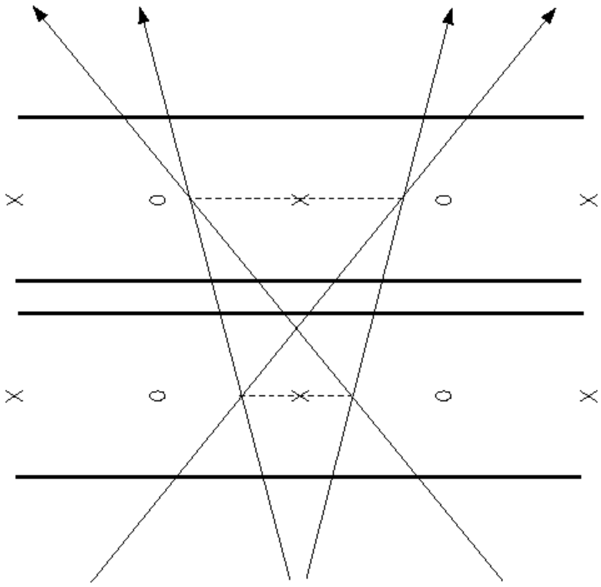

Figure 5: Representation of two identical MWDCs and the possible ambiguities in the true charged particle path. Each of the four rays constructed in this figure have the same value of χ^2 from a two-point fit.

For this test stand, the appropriate combination of drift distances and wires will be determined from the four X and four Y chambers in two separate reconstruction subroutines (see Appendicies A and B). These rather time-consuming algorithms go through all possible track combinations (allowing for possible multiple hits within each wire plane) and determine the χ^2 value for the linear fit of each. The track with the minimum χ^2 value will be selected as the appropriate ray to associate with the charged particle that triggered the event. This procedure will be carried out in the same manner in both the X chambers and the Y chambers. Each reconstruction subroutine should require that at least three chambers with valid drift times are present to proceed through the combinatorics analysis.

Studies of charged particle tracking through a similar detector stack that I have constructed, indicate that track selection based on a minimum χ^2 selects out the correct track roughly 90% of the time in a fit where four planes are present, and roughly 80% of the time when only three planes are present. However, the majority of the drift distance sign errors (misidentification of the correct side of the anode wire) occur in planes with small drift times, and thus these errors in a single plane do not adversely affect the resolution.

The tracking software will require a minimum number of planes for a good track fit of N=3, where N is the number of planes in each dimension with a hit. In order to determine the probability of having at least 3 out of 4 planes for either X or Y, we can use the binomial probability distribution:

$$P_B(x, n, p) = \frac{n!}{x!(n-x)!} p^x (1-p)^{n-x}. \tag{1}$$

Here P_B is the probability of observing x planes out of n in the event. The efficiency of each detector is given by p. If we assume that each wire plane in the test stand has an efficiency of 95% (a typical value), then the probability of observing at least 3 of 4 planes is given by:

$$\mathcal{P} = P_B(3, 4, 95\%) + P_B(4, 4, 95\%) = 98.6\%. \tag{2}$$

Thus the probability of having at least 3 of 4 planes in both the X and Y directions (again assuming a single plane efficiency of 95%) is 97.2%.

3 Tracking Software Parameters

There are a number of parameters that are crucial to define accurately for the tracking software. These include both geometrical and time-to-distance calibration parameters. The primary parameters include:

- Measured chamber wire plane Z locations (vertical coordinates).
  - The convention (defined in Fig. 6) is to denote (top to bottom) the X planes with Z_1, Z_2, Z_5, and Z_6 and the Y planes with Z_3, Z_4, Z_7, and Z_8.
- Measured wire offsets relative to X_0 and Y_0 (horizontal coordinates).
  - If the chamber stack is aligned as in Section 4, there should be only two global horizontal positioning parameters required to define the wire positions of all X and Y test stand chamber wires.
- Time distribution limits t_0 and t_{max}.
  - t_0 is the $t = 0$ value of the drift time.
  - t_{max} is the maximum value of the drift time within the drift cell.
  - The time limits may be defined separately for each chamber, for each 2735 preamp/discriminator card, or for each wire. The number of these parameters required depends on the uniformity of the chamber response.

4 Chamber Alignment

Before beginning the test stand chamber calibration, the chamber alignment must be fully understood in order to locate the upper two X (Y) planes relative to the lower two X (Y) planes (see Fig. 1). Note that the nominal position of each wire within the test stand chambers is indicated by a scribe mark on the aluminum case along the length of the chambers. (The accuracy of these marks has not been studied as this time.)

To begin the alignment procedure, the X chambers should be matched up, as shown in Fig. 6, such that the edges of the chambers both lie within the same vertical plane. This alignment should be carried out to better than 1 mm along the full extent of the chambers. This edge can be used to define the global horizontal offset parameter X_0. Each of the two X chambers should also be leveled such that the wires all lie in a horizontal plane. The same procedure must then be completed for the two sets of Y chambers (thus defining the second global horizontal offset parameter Y_0). It is important to ensure that the X chambers and the Y chambers are at 90° with respect to each other. If the test stand chamber support table is found to be square, the chamber frames can be measured (and located) with respect to its edges. Once the chamber stack has been positioned, the chambers must be locked into place. To avoid repeating the alignment procedure (and all subsequent calibrations), care must be taken to ensure that the chambers are not moved from their aligned positions.

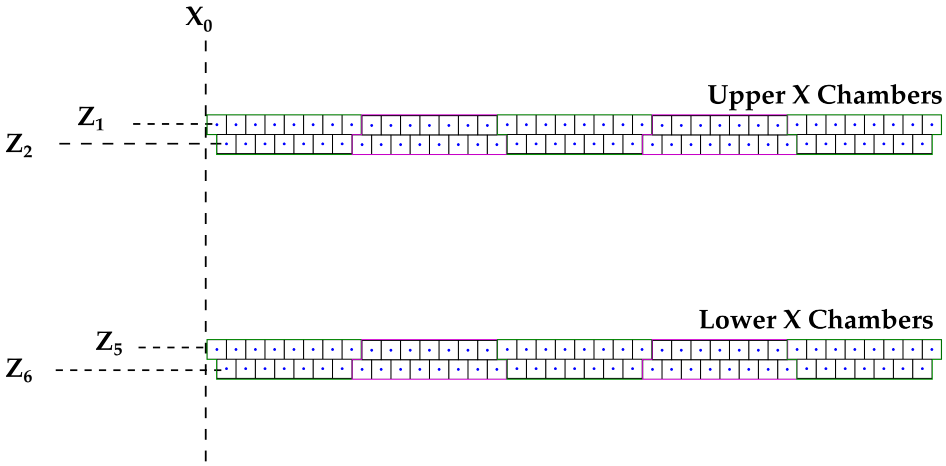

Figure 6: Layout of the X chambers of the cosmic ray test stand (the Y chambers are not shown). The geometry parameters X_0 (global horizontal offset) and Z_i (longitudinal stack positions) are defined. Note that neighboring drift chamber packages are colored differently.

Once the alignment procedure has been completed, the Z locations of the chambers can then be measured. This measurement should also be done with an accuracy of ~1 mm. In Fig. 6, the Z coordinates of the X chambers are labeled as Z_1, Z_2, Z_5, and Z_6. The corresponding Z coordinates of the Y chambers will then be Z_3, Z_4, Z_7, and Z_8. We can initially assume the following relations:

$$\begin{aligned} Z_2 &= Z_1 + 1.0 \qquad \text{(units in inches)} \\ Z_4 &= Z_3 + 1.0 \end{aligned}$$

$$
\begin{aligned}
Z_6 &= Z_5 + 1.0 \\
Z_8 &= Z_7 + 1.0.
\end{aligned} \tag{3}
$$

Procedures should be devised to double check all measurements for accuracy and uncertainties should be estimated. Fine tuning of the test stand chamber geometry parameters will have to be done during the stack calibration (see Section 5).

The wire locations for the X and Y chambers are fixed to first approximation once X_0 and Y_0 are measured. The position of each wire (i) is given by:

$$
\begin{aligned}
XPOS_{1,3}(i) &= X_0 + 0.5 \cdot i \qquad \text{(units in inches)} \\
XPOS_{2,4}(i) &= X_0 + 1.5 \cdot i \\
YPOS_{1,3}(i) &= Y_0 + 0.5 \cdot i \\
YPOS_{2,4}(i) &= Y_0 + 1.5 \cdot i,
\end{aligned} \tag{4}
$$

where planes $1 \rightarrow 4$ are numbered from top to bottom and assuming X_0 and Y_0 are defined from the edge of the chamber case as shown in Fig. 6. For planes $X1$ ($Y1$) and $X3$ ($Y3$), wire numbers run from 1 to 40; for planes $X2$ ($Y2$) and $X4$ ($Y4$), wire numbers run from 1 to 35. The Z positions of the wire planes are also indicated in Fig. 6.

5 Drift Time Calibration

In order to provide the required accuracy for the resolution studies, the chambers in the test stand must be properly calibrated. After the chamber alignment procedure has been completed (see Section 4), the drift time to drift distance calibrations must be determined. The calibration of the drift chambers will employ the raw TDC drift time information for each chamber (a representative spectrum is shown in Fig. 7), shifted by an offset parameter (t_0) to place the edge of the time range at t=0. As the average velocity of the secondary drift electrons is expected to be constant in the plane of the anode wires (where $v_d = dN/dt$), the drift time distributions, which represent the number of events recorded (dN) as a function of drift time (dt) across the extent of the drift cell, can be utilized to calculate the distance interval, ΔS, traveled by these electrons in any time interval Δt:

$$\Delta S = \frac{dN}{dt} \cdot \Delta t = \left(\frac{dS}{dN}\right) \cdot \left(\frac{dN}{dt}\right) \cdot \Delta t. \tag{5}$$

This expression of the chain-rule can be directly integrated over time to yield the distance S from the anode wire (t=0) to the origin of the ionizing event ($t = t_i$):

$$S(t_i) = \int_0^{t_i} \left(\frac{dS}{dN}\right) \cdot \left(\frac{dN}{dt}\right) \cdot dt \quad = \quad S_n \cdot \frac{\sum t_i}{\sum t_{max}}. \tag{6}$$

In this last expression, $\sum t_i$ represents the value of the drift time integral over the range from t=0 to $t = t_i$, and $\sum t_{max}$ represents the value of the integral over the full drift time distribution from t=0 to $t = t_{max}$, corresponding to the full extent of the drift cell S_n (where S_n=0.5 in).

Within the reconstruction software, this calibration can take the form of a look-up table. The integration of the drift time distribution can be performed for each 0.5 ns bin (the LSB resolution of the TDCs) from t=0 to $t = t_{max}$, and the resulting drift distances stored into an array which can be referenced for each event.

The steps in the calibration are then simply:

- Apply timing offsets t_0 for each channel to align the drift time spectra such that its leading edge is at zero.
- Integrate the drift time spectrum from 0 to t_{max}. Call this value INT_{full}.
- Integrate the drift time spectrum bin-by-bin from 0 to t_{bin}, with a granularity given by the LSB of the TDCs. Each of these values is called INT_{bin}.
- A lookup table can then be created with the values INT_{bin}/INT_{full} for each bin in drift time.
- The TDC value (or bin value) for a given measurement can then be converted to a drift distance using the known cell size for the test stand chambers (0.5 in) via:

$$dX = \frac{INT_{bin}}{INT_{full}} * \text{cell size}. \tag{7}$$

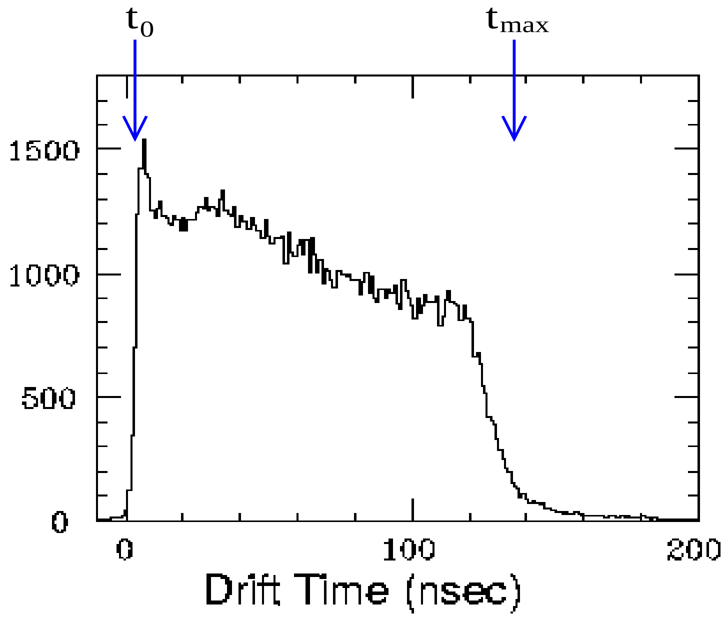

Figure 7: Representative drift time distribution for a typical horizontal drift chamber with a similar electrode structure to the test stand chambers showing the definitions of t_0 and t_{max}.

The calibration can be optimized by studying the fit residuals ($R \equiv X_{meas} - X_{calc}$) in the multi-layer fit. Changes in t_0 can be made to center the residual distributions about zero. Distributions of the drift distance vs. fit residual will be rotated if t_{max} is set too high or too low. Figs. 8 and 9 highlight some examples of residual distributions from a chamber stack with four wire planes and one half the cell spacing of the cosmic ray test stand chambers.

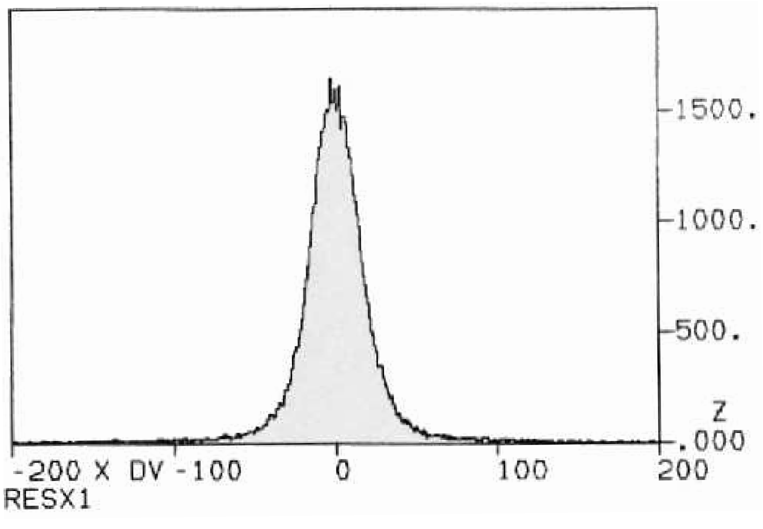

Figure 8: Residual distribution (in μm) in a chamber stack with four wire planes with one half the cell spacing of the cosmic ray test stand chambers using the all-but-one fitting method, i.e. showing the residual distribution in the excluded plane.

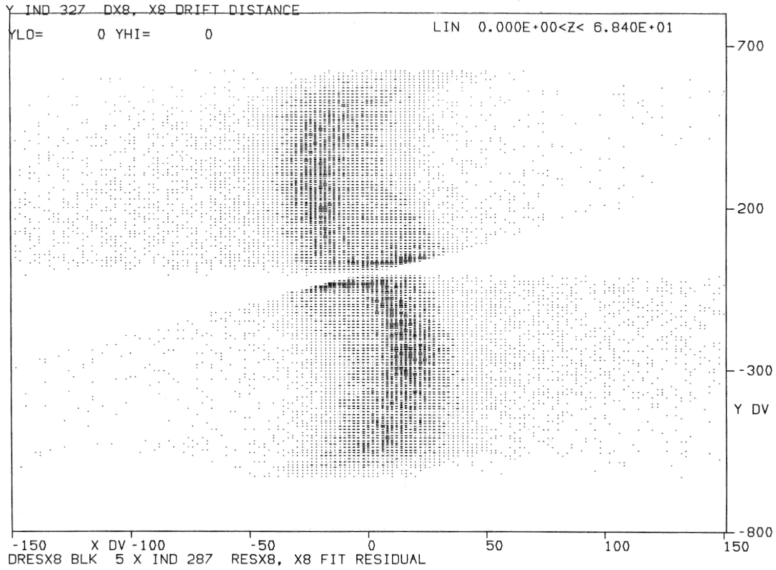

Figure 9: Drift distance distribution vs. fit residual (in μm) in a chamber stack with four wire planes with one half the cell spacing of the cosmic ray test stand chambers. Tilts and calibration non-linearities are clearly apparent.

The sensitivity to the individual chamber geometries and calibration parameters is heightened using a fit that excludes one plane at a time from the fit. Thus for the cosmic ray test stand where there are 4 X planes and 4 Y planes, the fits can be done for 3 planes at a time and then compared to the residuals in the excluded plane. This is typically referred to as an "all-but-one" fit.

The calibration is very sensitive to the choices of t_0 and t_{max}. Errors in these parameters typically introduce large correlations between the fit residuals (R) and the drift distances. Of course any correlations smear out the position resolution of the measurement.

The second phase of the MWDC calibration will involve optimizing the stack geometry parameters (X_0, Y_0, Z_i). As discussed in Section 4, the relative distance between the first wire in each plane and the edge of the aluminum chamber case must be measured in order to fully determine the relative wire positions from chamber to chamber. Errors in X_0 and Y_0 will appear as shifts of the residual distributions away from zero, and to a lesser extent, as increased widths, both of which increase the angular uncertainty. The procedure for finalizing the transverse MWDC geometry parameters will be to adjust the software X_0 and Y_0 parameters of the individual wire chambers until the fit residual distributions are each centered about zero. These offset adjustments should be within the measurement uncertainties.

Errors made in the longitudinal stack geometry parameters (Z_i) will lead to a broadening of the residual distributions and perhaps a non-Gaussian component. To set the final Z_i chamber parameters, these offsets should be adjusted within the measurement uncertainties until the optimal resolution is achieved.

6 Track Residuals

Using the "all-but-one" method detailed in Section 5, there are two levels of fit residuals R that can be studied. Initially, before the time-to-distance calibration is completed, crude track residuals R_C can be computed. These are defined as:

$$R_C = \text{wire position} - \text{crude track point}, \tag{8}$$

where,

- wire position - location of the hit wire relative to X_0 for the X chambers or Y_0 for the Y chambers.
- crude track point - from least squares fit to the hit wire locations.

The procedure is to define a track via "hit-based" tracking. However, after the time-to-distance calibration has been included, a more sensitive level of "time-based" tracking can be performed. This enables computation of a full track residual R_F, defined as:

$$R_F = \text{hit position} - \text{fit track point}, \tag{9}$$

where,

- hit position - location of the hit wire ± dX relative to X_0 for the X chambers or Y_0 for the Y chambers .
- fit track point - from least squares fit to the hit positions.

The width of the full track residual R_F is a direct measure of the position resolution of the cosmic ray test stand system.

7 Calibration Diagnostics

The histogram of drift distance vs. residual provides a powerful diagnostic for the time-to-distance calibration of the chambers. In this section the effect of the four basic calibration parameters, time offsets (t_0), drift velocity (mediated through t_{max}), global transverse chamber position offsets (X_0,Y_0), and wire errors, are discussed in relation to their affect on the drift distance vs. residual plots.

7.1 Time Offsets

The time offset t_0 is the parameter that sets the $t = 0$ location of the drift time distribution. The nominal drift time distribution reflects the electron drift time over the full extent of the drift cell, from the location of the anode wire ($t = 0$) to the cathode ($t = t_{max}$). A typical drift time distribution for an MWDC (with cell spacing one half that of the cosmic ray chambers) is shown in Fig. 7. Fig. 10 shows the effect of different t_0 values on the drift distance vs. residual plots. Setting the time offsets t_0 is important to do accurately because the main contributions to the integral in Eq.(5) come from those channels near t_0. If t_0 is too large, we cut off channels affecting the drift velocity. It t_0 is too small, we leave a gap in the drift distance distribution that manifests itself as multiple peaking (see Fig. 11).

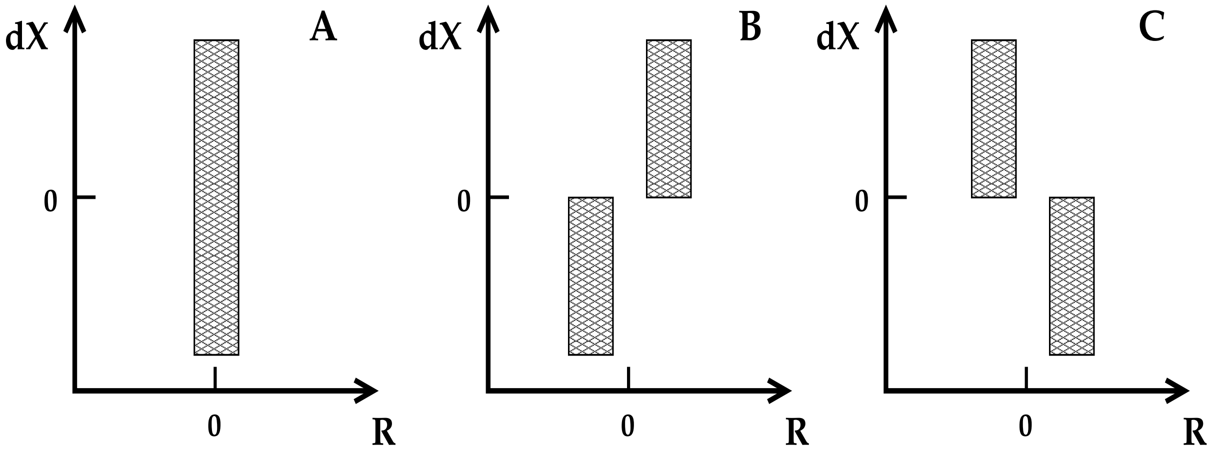

Figure 10: Distributions of drift distance vs. residual showing the effect of the time offset t_0 on the distributions. A): Nominal t_0, B): t_0 too small, C): t_0 too large.

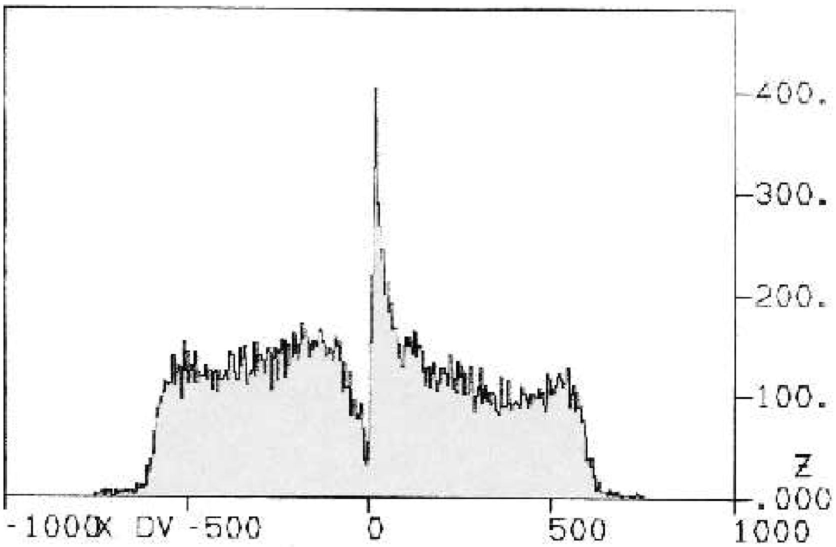

Figure 11: Drift distance distribution (in μm) for a chamber with one half the cell spacing of the cosmic ray test stand chambers. The dip/spike structure near zero drift distance is due to a slight problem with the specification of the t_0 parameter.

7.2 Drift Velocity

Fig. 12 shows a plot of drift distance vs. drift time for three different values of the gas drift velocity. Here it is assumed that $v_{d3} < v_{d2} < v_{d1}$. Given that the drift distance is given by:

$dX =$ drift time $\cdot\, v_d$ the longer the drift time, the larger the error made for an error in the assumed drift velocity. Thus the residual $R = f(dt) = f(dX)$.

The value of the drift velocity is assumed by the selection of t_{max}, the maximum drift time (see Fig. 7). Selection of t_{max} that is too large (small) results in a smaller (larger) assumed drift velocity v_d. Fig. 13 shows how the plots of drift distance vs. residual are affected by having the drift velocity v_d too small or too large. Note that any non-linearities in the drift time to drift distance calibration will appear as curves and wiggles in these rotated plots (see Fig. 9).

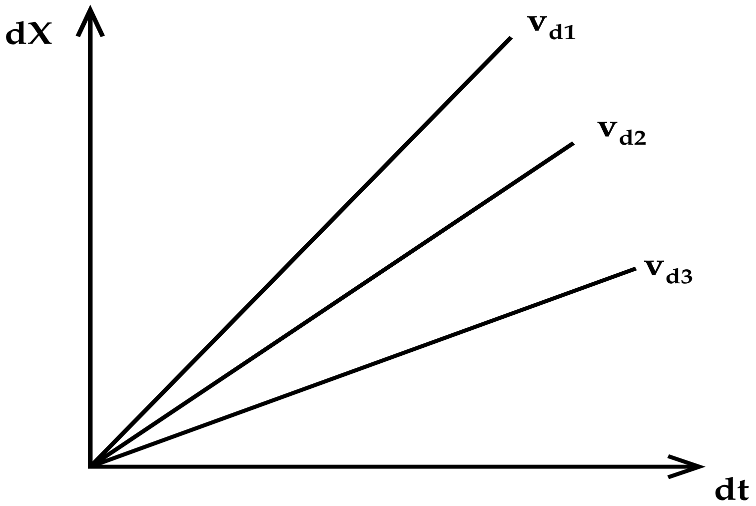

Figure 12: Plots of drift distance vs. time for three different values of the gas drift velocity where $v_{d3} < v_{d2} < v_{d1}$.

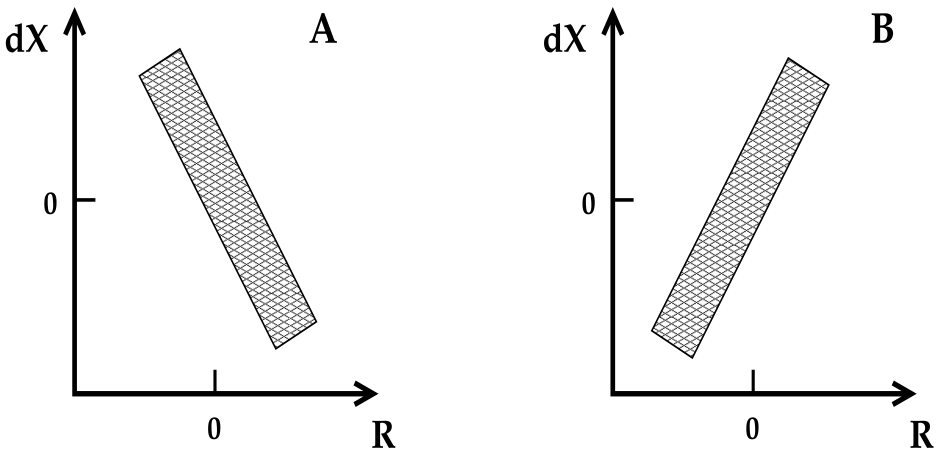

Figure 13: Distributions of drift distance vs. residual showing the effect of (A): having v_d too small and (B): having v_d too large.

7.3 Transverse Offsets

A single position coordinate X_0 for the X chambers or Y_0 for the Y chambers is used to locate the wires in a given wire plane. The location of each wire in the plane, i.e. the transverse coordinate of each wire (i), is then given by:

$$
\begin{aligned}
X_i &= X_0 + \Delta X_i \\
Y_i &= Y_0 + \Delta Y_i.
\end{aligned}
\tag{10}
$$

If the transverse offset parameter (X_0 or Y_0) is incorrect for a given chamber (relative to the others in the stack), the residual distributions will be systematically shifted as shown in Fig 14.

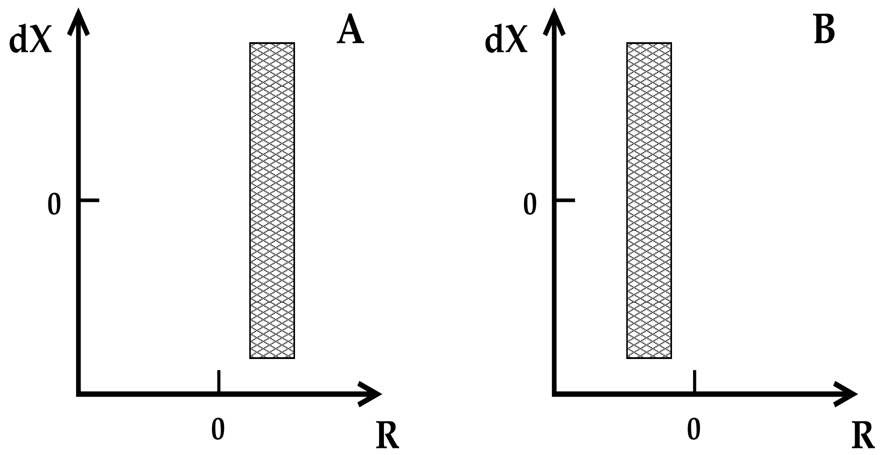

Figure 14: Distributions of drift distance vs. residual showing the effect of (A): having X_0 too small and (B): having X_0 too large.

7.4 Wire Errors

It is possible for neighboring drift cells in a given wire layer to potentially fire. Typically this can happen for charged particles passing very close to the boundary of two drift cells. In these situations there is a reasonable probability to use the wrong drift cell in the computation of the track residual (i.e. use the wrong wire offset in Eq.(10)) above. The manifestation of this type of error in the drift distance vs. residual plot is the non-central regions labeled A, B, C, and D in Fig. 15.

Fig. 16 shows a schematic picture of a charged particle passing through a series of drift planes. The appropriate drift distances are indicated in green. For wire layer #1, the possible errors in wire identification are shown and labeled with the portion of the space in Fig. 15 that they will occupy.

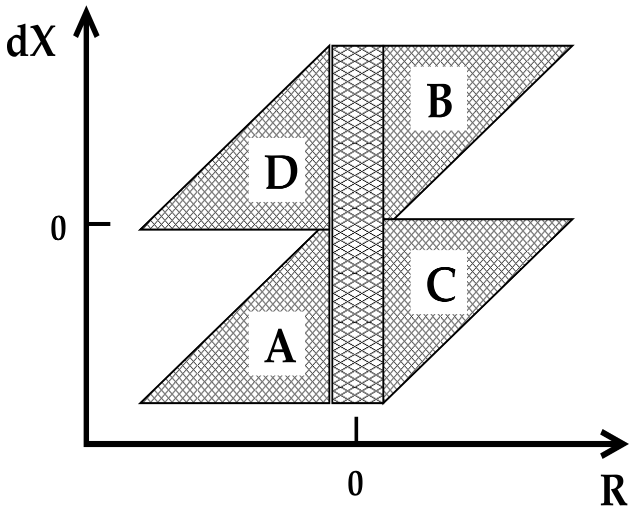

Figure 15: Distributions of drift distance vs. residual showing the effect of wire errors populating the non-central regions labeled A, B, C, and D.

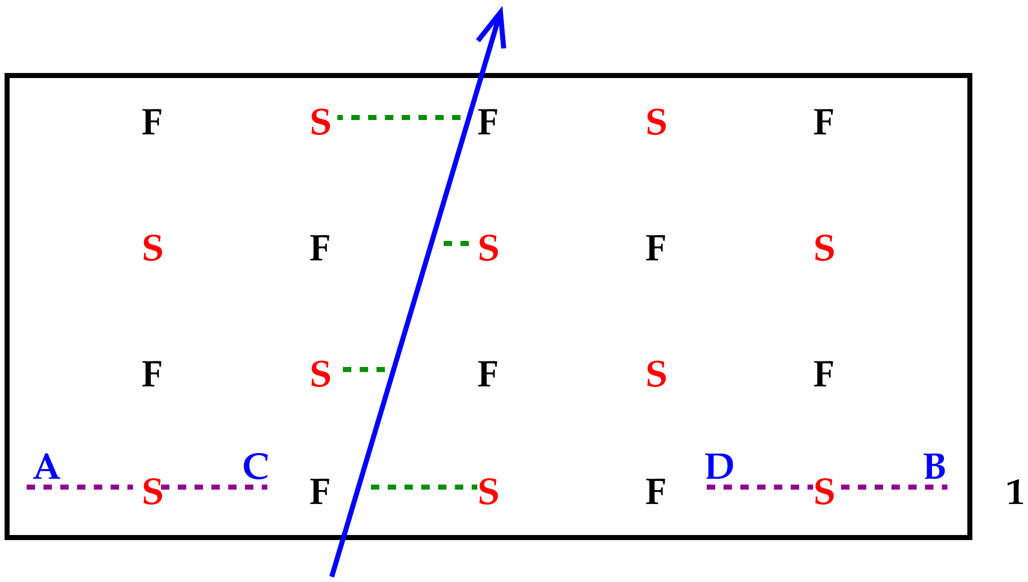

Figure 16: Schematic picture of a charged particle tracking passing through a series of drift planes. The true drift distances are denoted in green. The corresponding errors and the portion of the space in Fig. 15 occupied is labeled for wire layer #1. Here S represents a sense wire and F represents a field wire or the cathode.

8 Current Progress

To this point in time (June 2004) we have managed to readout two groups of 16 channels from the cosmic ray test stand chambers. This amount to two of the chambers, each readout by a single LeCroy 2735 preamplifier/discriminator card. Some of the data is included in Figs. 17 - 20. These data were acquired with a 90% Argon - 10%CO_2 gas mixture and a discriminator threshold voltage set at 5.0 V. The chambers were set at an operating voltage of -2100 V on the anode wires and the cathodes were grounded. The data acquisition rate was on the order of 1 Hz and data was acquired for about 15 minutes.

The timing information from each wire was encoded with LeCroy 1877 96-channel TDCs operated in common stop mode. The TDC stop was provided by the trigger scintillator overlap, and the TDC starts were provided by the signals from the individual wires. The TDCs allowed for the recording of both the leading and trailing edges of each ECL logic pulse from the preamplifier card. The width of this pulse is a direct measure of the time over threshold of the preamplifier card signal. This measurement proved extremely useful in distinguishing between true charged particle related chamber hits, and signals resulting from noise or cross-talk. These unwanted signals are characterized by very narrow ($\leq$ 30 nsec) pulses and were eliminated employing a software gate.

Fig. 17 shows the preamplifier time over threshold (pulse width) distribution for the channels readout. Pulses less than 30 ns (trailing - leading edge time difference) are entirely due to noise and cross-talk related signals from the chambers.

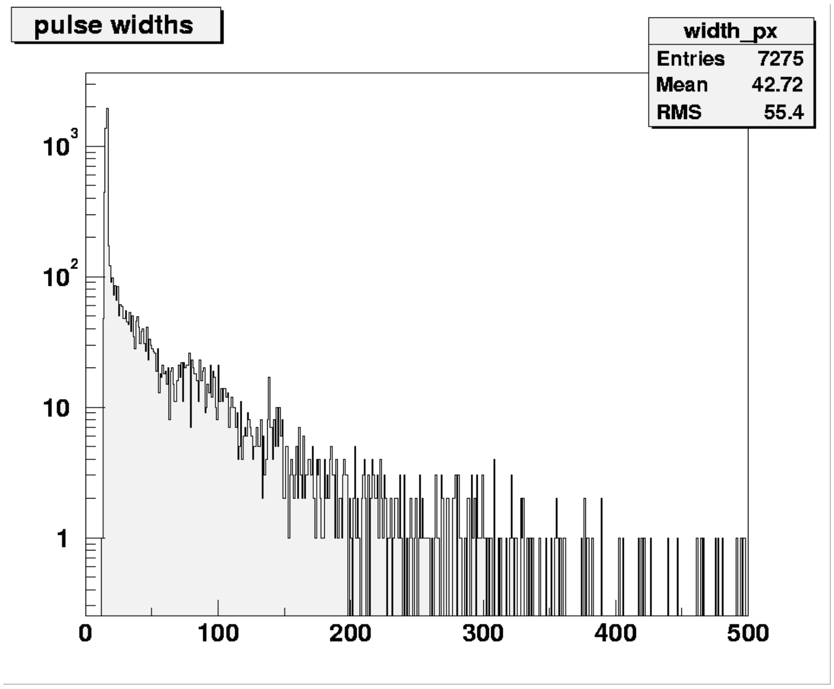

Figure 17: Preamplifier time over threshold signal from one of the cosmic ray test stand chambers. This so-called pulse width distribution can be used to eliminate noise and cross-talk related signals from the chambers.

Fig. 18 shows the distribution of TDC channel number vs. leading edge times for the channels readout. This spectrum has no cut on the pulse width and is totally dominated by noise. Fig. 19 shows the same distribution with a pulse width cut at 30 nsec. At this point a reasonable drift time distribution emerges from the spectrum. This is seen more clearly as a projection on the time axis in Fig. 20.

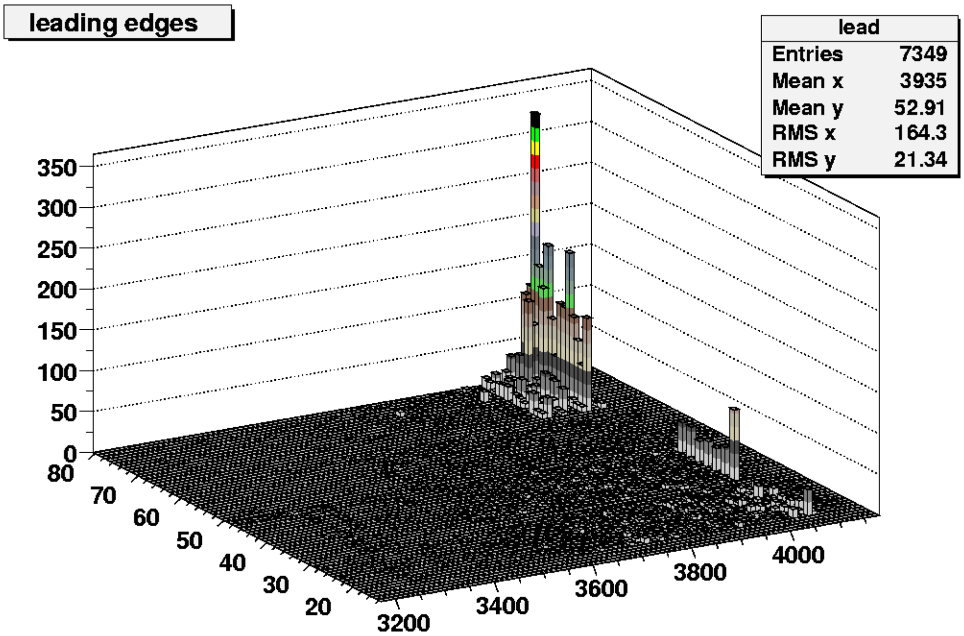

Figure 18: Distribution of TDC channel number vs. leading edge times for one of the cosmic ray test stand chambers. This spectrum, with no pulse width cut, is totally dominated by noise pickup on the chamber electronics.

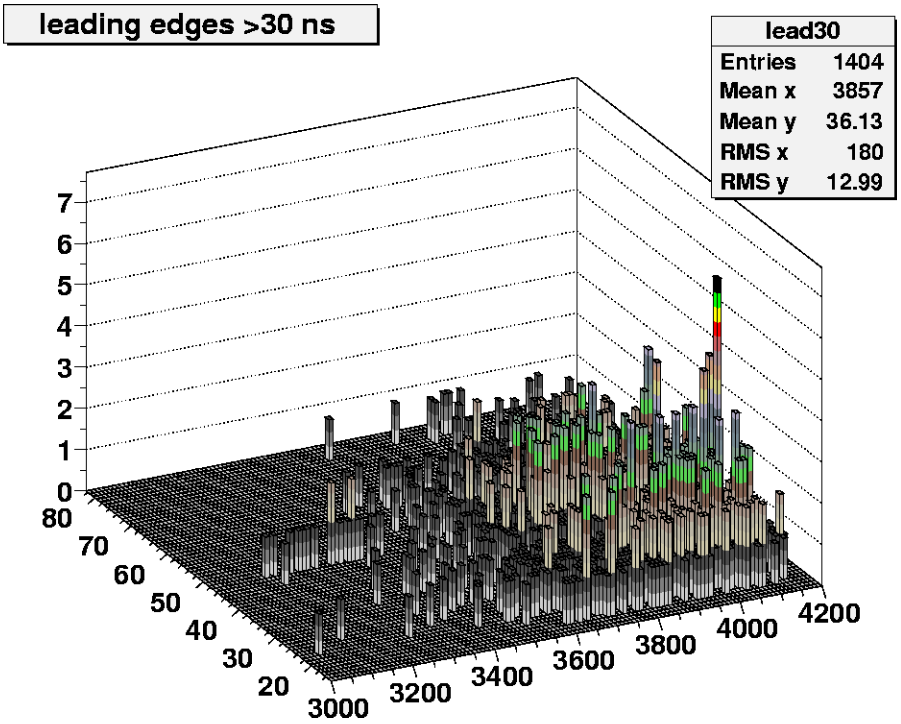

Figure 19: Distribution of TDC channel number vs. TDC leading edge time for one of the cosmic ray test stand chambers after application of a pulse width cut of 30 ns (see Fig. 17).

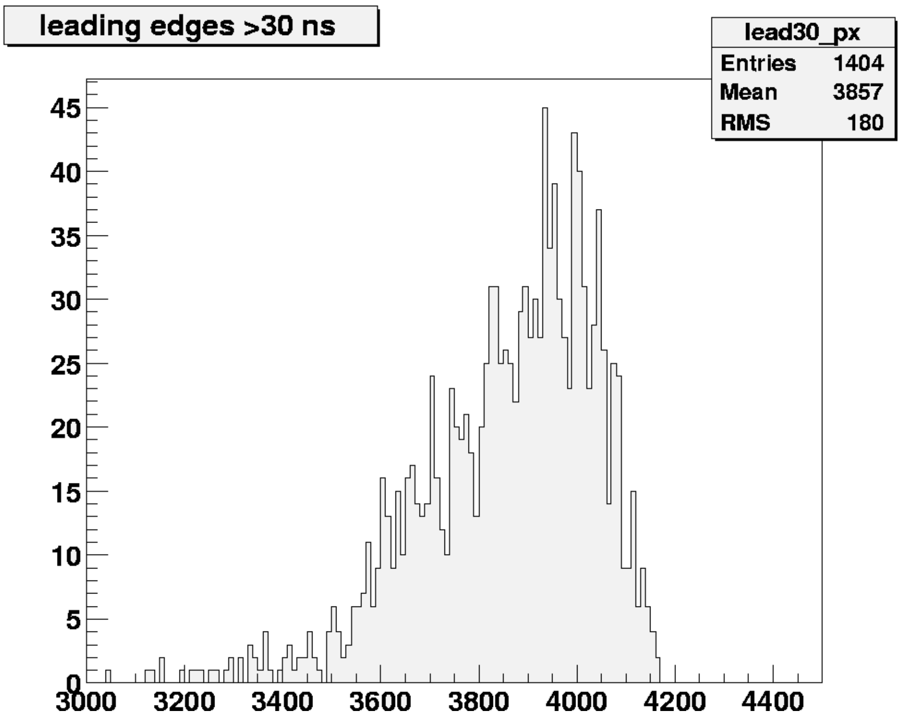

Figure 20: Distribution of TDC leading edge times for one of the cosmic ray test stand chambers after application of a pulse width cut of 30 ns. This plot is a projection of Fig. 19 onto the time axis. What is seen (with low statistics) is a drift time distribution. As the chamber readout is in common stop mode, longer drift times appear at smaller channel numbers.

Appendix A - Track Fitting Routine

```
c
c  Enter X nested DO loop.  Test all possible combinations of drift distance
c  signs in each wire plane.  Search for the minimum chi**2 value.
c
   chixmin=1.e35
   do n1=1,2
      xpt(1)=wposx(1)+sign(n1)*dx(1)
      do n2=1,2
         xpt(2)=wposx(2)+sign(n2)*dx(2)
         do n3=1,2
            xpt(3)=wposx(3)+sign(n3)*dx(3)
            do n4=1,2
               xpt(4)=wposx(4)+sign(n4)*dx(4)
c
c  Fit track then calculate and test the value of chi**2.
c
               call linfit(z1,xpt,sigx,xvar,1,sxz,exz,xint,exint)
               chix=0.0
               do k=1,4
                  resx(k)=xpt(k)-(sxz*z1(k)+xint)
                  chix=chix+resx(k)**2
               enddo
               if (chix.le.chixmin) then
                  do k=1,4
                     xpt_tmp(k)=xpt(k)
                     resx_tmp(k)=resx(k)
                  enddo
                  xintmin=xint
                  sxzmin=sxz
                  chixmin=chix
               endif
            enddo
         enddo
      enddo
   enddo
```

Appendix B – Least Squares Fit Routine

```
    subroutine LINFIT(x,y,sigmay,npts,mode,b,sigmab,a,sigmaa)
       real*8 sum, sumx, sumy, sumx2, sumxy, sumy2
       real*8 xi, yi, weight, delta, varnce
       real*4 x(4),y(4),sigmay(4), b, a, sigmab, sigmaa
        integer*4 npts,mode
c
c  Accumulate weighted sums.
c
   11  sum = 0.
       sumx = 0.
       sumy = 0.
       sumx2 = 0.
       sumxy = 0.
       sumy2 = 0.
   21  do 50 i=1,npts
          xi = x(i)
          yi = y(i)
          if (mode) 31, 36, 38
   31     if (yi) 34, 36, 32
   32     weight = 1./yi
          go to 41
   34     weight = 1./(-yi)
          go to 41
   36     weight = 1.
          go to 41
   38     weight = 1./sigmay(i)**2
   41     sum   = sum   + weight
          sumx  = sumx  + weight*xi
          sumy  = sumy  + weight*yi
          sumx2 = sumx2 + weight*xi*xi
          sumxy = sumxy + weight*xi*yi
          sumy2 = sumy2 + weight*yi*yi
   50  continue
c
c  Calculate coefficients and standard deviations.
c
   51  delta = sum*sumx2 - sumx*sumx
       a = (sumx2*sumy - sumx*sumxy)/delta
   53  b = (sumxy*sum - sumx*sumy)/delta
   61  if (mode) 62, 64, 62
   62  varnce = 1.
       go to 67
   64  c = npts - 2
```

```
    varnce = (sumy2+a*a*sum+b*b*sumx2 -2.*(a*sumy+b*sumxy-a*b*sumx))/c
67  sigmaa = dsqrt(varnce*sumx2/delta)
68  sigmab = dsqrt(varnce*sum/delta)
71  r = (sum*sumxy-sumx*sumy)/dsqrt(delta*(sum*sumy2-sumy*sumy))
return
end
```

References

[1] D.S. Carman, "Hall D Forward Drift Chamber Prototype Test Plan", see URL http://www.phys.cmu.edu/halld/halld_notes/index_notes.html.

[2] See the LeCroy 2735DC and 2735PC data sheets on the web at URL http://www.lecroy.com/lrs/dsheets/2735.htm.